NANO LETTERS

pubs.acs.org/NanoLett
Letter

Rolling Motion of Rigid Skyrmion Crystallites Induced by Chiral Lattice Torque

Haonan Jin, Jingyi Chen, Gerrit van der Laan, Thorsten Hesjedal, Yizhou Liu,* and Shilei Zhang*

Cite This: *Nano Lett.* 2024, 24, 12226−12232

ABSTRACT: Magnetic skyrmions are topologically protected spin textures with emergent particle-like behaviors. Their dynamics under external stimuli is of great interest and importance for topological physics and spintronics applications alike. So far, skyrmions are only found to move linearly in response to a linear drive, following the conventional model treating them as isolated quasiparticles. Here, by performing time and spatially resolved resonant elastic X-ray scattering of the insulating chiral magnet Cu_2OSeO_3, we show that for finite-sized skyrmion crystallites, a purely linear temperature gradient not only propels the skyrmions but also induces continuous rotational motion through a chiral lattice torque. Consequently, a skyrmion crystallite undergoes a rolling motion under a small gradient, while both the rolling speed and the rotational sense can be controlled. Our findings offer a new degree of freedom for manipulating these quasiparticles toward device applications and underscore the fundamental phase difference between the condensed skyrmion lattice and isolated skyrmions.

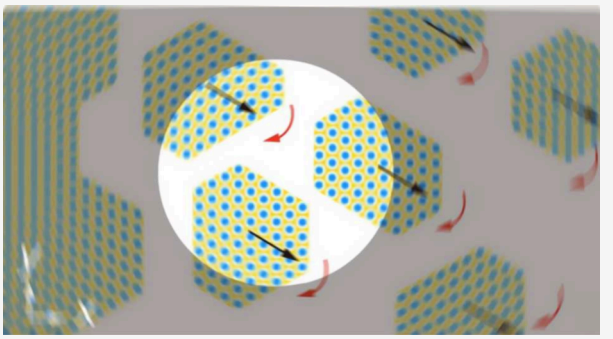

KEYWORDS: *magnetic skyrmions, skyrmion dynamics, topological magnetism, resonant elastic X-ray scattering, temperature gradient*

Magnetic skyrmions are topologically ordered spin textures that present particle-like properties.[1−3] They are found to induce novel emergent physics[4−7] and are proposed as promising information carriers for spintronics devices.[8−11] While the understanding of the skyrmion dynamics is of great importance for topological magnetism, current studies are based on the "single-particle" model, i.e., the steady-state motion of a single skyrmion as described by the Thiele equation.[12] In essence, isolated skyrmions pick up a linear velocity under external driving stimuli such as electric current,[10,13−18] thermal[19−30] or magnetic field gradients.[31,32] Consequently, they travel along a linear path (Figure 1a), which employs a temperature gradient drive as an example.

In certain materials such as chiral magnets, skyrmions prefer to condense into closely packed two-dimensional hexagonal lattices, i.e., the skyrmion lattice (SkL) phase.[2,33−36] The quasiparticle crystallization suggests that the interskyrmion correlation[20,37−43] plays a role, leading to an ordered phase. In fact, the lattice state should be regarded as a distinct phase compared to isolated skyrmions, in analogy to the distinction between the solid and liquid phase of a physical system.[44,45] The immediate consequence of broken rotational symmetry for an ordered phase is lattice rigidity,[45,46] i.e., a block of the correlated skyrmion crystal prefers to stay as an entity, and resists to be broken up into isolated particles. Hence, the driven dynamics of a finite-sized skyrmion lattice crystallite (SkC) is expected to be fundamentally different from that of

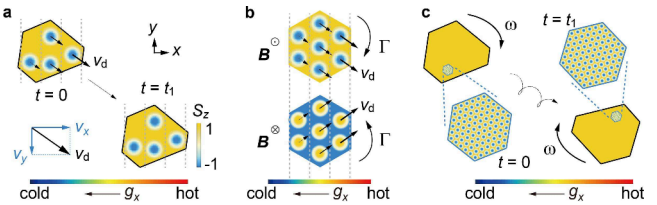

Figure 1. Comparison of the dynamical responses of an ensemble of isolated skyrmions and a rigid skyrmion lattice under a linear temperature gradient along x. (a) Ensemble of isolated skyrmions undergoing translational motion. The local drift velocity $\mathbf{v}_d$ is composed of v_x, which is parallel to the gradient, and v_y, which is due to the skyrmion Hall effect and perpendicular to the gradient. Additionally, the spatially varying temperature leads to a velocity difference along x. As a consequence, isolated skyrmions collectively move toward the bottom-right direction, following linear paths. (b) In contrast, if the skyrmions condense into a closed-packed, hexagonally ordered lattice, the velocity inhomogeneity across the entire domain leads to a net torque, thus driving the SkC to rotate with a fixed chirality and a uniform drift velocity. Note that the torque reverses its direction when the magnetic field direction is reversed. (c) On a large scale, a finite-sized SkC exhibits simultaneous translational and rotational motion, following a rolling trajectory.

Received: July 15, 2024
Revised: September 10, 2024
Accepted: September 17, 2024
Published: September 19, 2024

https://doi.org/10.1021/acs.nanolett.4c03336
Nano Lett. 2024, 24, 12226−12232

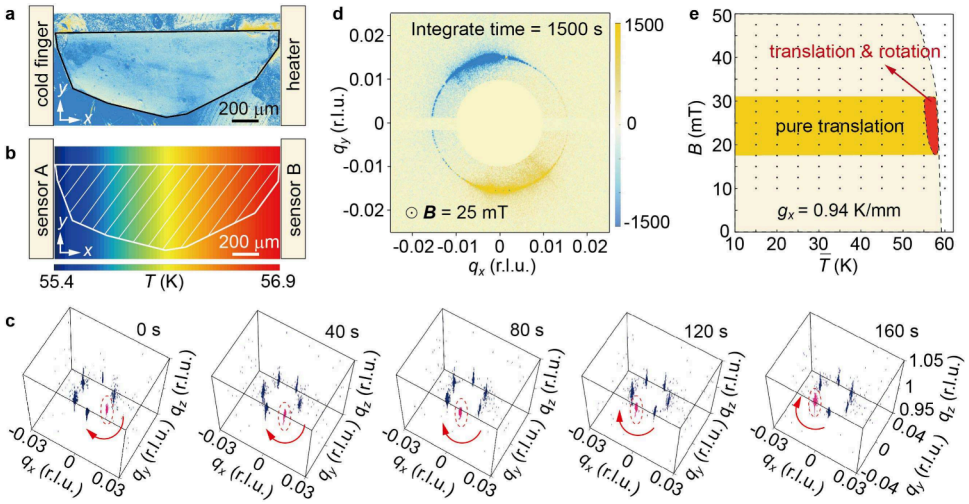

Figure 2. Observation of the SkC rotation under a linear temperature gradient. (a) SEM image of the measured sample on the temperature gradient holder, incorporating a heater and temperature sensors at both ends. (b) Linearly approximated temperature distribution across the sample with $\bar{T} = 56.15$ K and $g_x = 0.94$ K/mm, at which the skyrmions rotate. The applied field is $B_z = 25$ mT. (c) 3D-RSM patterns recorded at 40 s time intervals as indicated. The duration of each individual measurement is 2 ms. (d) Time-integrated CD-REXS map of the rotating skyrmion patterns, revealing a measured surface twist helicity angle of 150°. (e) $(\bar{T}, B)$-phase diagram for $g_x = 0.94$ K/mm. The equilibrium SkL phase pocket is marked in red. Here, both translational and rotational modes are present. The metastable SkL phase region (marked in yellow) is stabilized through rapid field-cooling. This phase pocket only exhibits translational dynamics.

isolated skyrmions, though these aspects are still at their early stages of exploration.[13,40]

It has been theoretically proposed that a rotational mode of the SkCs can be established by configuring a one-dimensional (1D), spatially inhomogeneous parameter, such as the damping constant α, dissipative tensor $\mathcal{D}$, or the modulus of the magnetization S.[20,47,48] The inhomogeneity can be experimentally achieved by a general linear gradient,[47,48] which results in an effective torque. As a consequence, a SkC will continuously translate and rotate. Nevertheless, such a torque-induced rotation was only observed in the metallic chiral magnet MnSi, where both electric current and temperature gradient have to be present at the same time.[13] Moreover, the SkC were only found to rotate by a finite angle, whereas the realization of its continuous rotation and translational motion remained elusive.

Here, by applying a purely linear temperature gradient, we uncover the existence of a *chiral lattice torque* that governs the dynamics of rigid SkCs, which leads to continuous rotational modes for the SkCs during their travel. Our time- and spatially resolved resonant elastic X-ray scattering (REXS) measurements were carried out on the insulating skyrmion-hosting material Cu_2OSeO_3, subjected to a 1D thermal gradient. For this insulating material, other possible sources of dynamics, such as inhomogeneous current distributions or current-induced Joule heating, can be ruled out, making it the ideal physical system for the quantitative study of skyrmion lattice dynamics.

In the chiral lattice torque model (see the Supporting Information for details), the steady-state motion of a rigid SkC can be written in terms of the collective coordinates $\mathbf{S}(\mathbf{r}, t) = \mathbf{S}_0[\hat{O}(\mathbf{r} - \mathbf{R}^{\mathrm{SkC}})]$, where $\mathbf{S}$ is the classical local spin vector that is defined in two-dimensional real-space $\mathbf{r} = (x, y)$, $\mathbf{S}_0(\mathbf{r})$ is the initial skyrmion lattice texture, $\mathbf{R}^{\mathrm{SkC}} = \mathbf{v}_d^{\mathrm{SkC}} t$ is the displacement of the entire crystallite, and $\mathbf{v}_d^{\mathrm{SkC}}$ is the collective SkC's drift velocity. A rotational operator $\hat{O}$ is introduced in order to account for the lattice rigidity, which vanishes for isolated (rotationally symmetric) skyrmions. For a chiral magnet, the presence of a linear temperature gradient $\mathbf{g} = \nabla T$ not only produces a unidirectional magnon current $\mathbf{j}_m \| \mathbf{g}$ that pushes the skyrmions toward the hot end,[19,22,26,29] but also results in a spatially varying spin length $S = |\mathbf{S}|$.[49] The latter suggests a nonvanishing term $\partial S/\partial T$, which essentially leads to a net torque $\mathbf{\Gamma}$ acting on the SkC.

A heuristic model that explains the origin of $\mathbf{\Gamma}$ is illustrated in Figure 1b. A linear temperature gradient g_x results in a magnon current j_x. Thus, each individual skyrmion experiences a local drift velocity $\mathbf{v}_d$, which is composed of v_x due to the dissipative force and v_y due to the Magnus force.[13,19,48,50,51] Importantly, a small, but finite $\partial S/\partial T$ leads to a spatially varying $|\mathbf{v}_d(x)|$,[48] i.e., the skyrmion Hall angle remains uniform, while the modulus of the drift velocity monotonically increases along x. Such an inhomogeneity in the velocities will lead to a separation of the skyrmions. However, for a condensed SkC, the cohesion between neighboring skyrmions is preserving the lattice rigidity, leading to a uniform $\mathbf{v}_d^{\mathrm{SkC}}$ of the entire quasiparticle ensemble. As a consequence, the local vectorial velocity along each edge of the crystallites differ from one another, resulting in a net torque $\mathbf{\Gamma}$ that essentially rotates the lattice with a finite angular velocity $\boldsymbol{\omega}$ (see SI Appendix), which can be written as

$$\boldsymbol{\omega} \approx \frac{1}{N\Omega} \frac{2\pi Q}{\alpha \mathcal{D}} \frac{\partial S}{\partial T} j_x v_x \tag{1}$$

where $Q = S \int \mathbf{S} \cdot (\partial_x \mathbf{S} \times \partial_y \mathbf{S})\, \mathrm{d}\mathbf{r}$ is the topological charge of an individual skyrmion, N is total number of skyrmions within the SkC, $\Omega = 0.0035\ \mu\mathrm{m}^2$ is the area of the primitive unit cell,[52] i.e., the area of the crystallite can be written as $N\Omega$.

Importantly, the sign of $\mathbf{\Gamma}$ is fixed by the relative orientations between the temperature gradient and the topological charge Q, thus presenting a *chiral lattice torque*. Therefore, by reversing the magnetic field, Q flips sign, leading to the opposite rotational sense (Figure 1b). Figure 1c illustrates a

https://doi.org/10.1021/acs.nanolett.4c03336
Nano Lett. 2024, 24, 12226−12232

finite-sized SkC as experienced in a typical experiment, which is much larger than the hexagonal cluster sketched in Figure 1b.[35,40,53,54] The large-scale SkC thus presents both translational and rotational dynamics, traveling in a rolling manner. The motivation for our experiment was hence to observe the signature dynamics of a skyrmion lattice under linear temperature gradients.

Resonant elastic X-ray scattering (REXS) was performed on Cu_2OSeO_3 subjected to a linear temperature gradient g_x. Figure 2a shows a scanning electron microscopy (SEM) image of the sample mounted on the temperature-gradient holder. The single-crystal has the shape of a thin slab and measures 1.6 × 0.6 × 0.1 mm^3. A well-polished [001] surface was mounted directly onto the goniometer holder,[36] assuring excellent thermal contact. Three-dimensional reciprocal space maps (RSMs) were obtained by varying the scattering angles (see *SI Appendix*, Methods, for details on the 3D RSM reconstruction).[55,56] Throughout the measurements, we use a 20 μm-diameter X-ray beam and a measurement time of 2 ms for each REXS pattern.

For the temperature setup, the cooling power is provided by a coldfinger at the left side of the holder, which realizes stable temperature control (i.e., ± 10 mK).[57] A heater diode is mounted on the right-hand side, establishing a linear thermal gradient along $-x$ by applying a small current to the diode. Two local temperature sensors are attached along the two sides, which monitor the temperatures in real-time. As shown in Figure 2b, using sensor A, the sample temperature is first controlled to obtain a homogeneous temperature configuration that stabilizes the SkL phase at an elevated field of B_z = 25 mT.[56] Subsequently, the diode current is switched on, producing a tunable g_x that is experimentally determined via the difference of the two temperature sensors A and B. We define the sample temperature as the spatially averaged temperature $\overline{T}$, and use the as-measured g_x to quantify the dynamic drive. Figure 2b shows our configured temperature gradient for $\overline{T}$ = 56.15 K and g_x = 0.94 K/mm, at which the real-time REXS measurement is carried out to monitor the dynamical response from the system.

In the conventional model, skyrmions would collectively travel along a linear path under g_x, following the translational mode (Figure 1a). Such a linear motion does not lead to a shape change in the REXS pattern as the scattering intensity in reciprocal space is insensitive to the relative phase of a SkL.[52] However, for the sample environment (Figure 2b), it is found that the REXS pattern surprisingly rotates. Figure 2c shows a series of snapshots of the RSM of the SkL phase under g_x = 0.94 K/mm. The entire 3D RSM pattern undergoes continuous rotation with a fixed chirality, i.e., clockwise, as shown by the tracked red rod (Figure 2c). This can be further seen by the time-integrated circular dichroic REXS (CD-REXS) pattern in (Figure 2d). 6-fold-symmetric magnetic crystalline truncation rods with finite length are identified, suggesting that a hexagonal skyrmion lattice is formed within the probing area at all times.[55] By performing the truncation rod analysis[55,56] (Section S1 in the Supporting Information), we are able to confirm that skyrmions form 3D tube-like structures. Furthermore, the well-defined dichroism reveals that the measured helicity angle[58] maintains a value of 150°, consistent with the static value of Cu_2OSeO_3 due to the surface twist effect.[58,59] Therefore, a continuous rotation of the SkC is realized under the purely linear temperature gradient.

Although the pattern rotates with a rather slow angular velocity of ω = 0.75°/s, the dynamic behavior responds sensitively to the external stimuli, i.e., the rotation immediately takes place once g_x is switched on, and stops once g_x is switched off. By increasing g_x, ω increases accordingly. There is a threshold value of g_x = 0.56 K/mm, below which the RSM pattern remains static. By reversing the polarity of the applied magnetic field, the rotation sense also reverses to be counterclockwise (Movie 2 in the Supporting Information), consistent with the chiral lattice torque model. The constant length of the truncation rods (Figure 2c), and the constant skyrmion helicity angle (Figure 2d), demonstrate that the observed dynamics is not governed by dynamic 3D effects,[55,56,58,59] e.g., the breaking/merging of skyrmion tubes (within the probing depth). Thus, our chiral lattice torque model that is based on the 2D properties of the skyrmions is applicable for our investigated system.

The rolling SkC behavior only occurs within the equilibrium SkL phase. Figure 2e shows the dynamical ($\overline{T}$, B) phase diagram for the as-measured sample by keeping g_x = 0.94 K/mm (heater turned on). Following by the rapid-cooling protocol,[60] the ordered SkL is observed to survive in a broadened temperature range (yellow region in Figure 2e). Nevertheless, under the same g_x, the RSM rotation instantaneously stops once $\overline{T}$ exceeds the equilibrium skyrmion lattice pocket boundary value (red region in Figure 2e). The dynamics is recovered once $\overline{T}$ re-enters the red pocket area. In the metastable SkL state, even though the time-dependent REXS data exhibits a fixed pattern, an oscillation of the magnetic peak intensity over time can be observed (Section S3 in the Supporting Information), suggesting that a number of SkCs are traversing across the X-ray probing area in a translational fashion. This reveals that the interskyrmion correlation for the equilibrium SkL is fundamentally different with the metastable phase, i.e., the quasiparticle crystallization may be more rigid for the equilibrium state. The absence of rolling motion can be understood as a consequence of the increased disorder, weaker lattice cohesion, and the presence of pinning effects. For instance, owing to their nucleation history, metastable skyrmions will be trapped in local energy minima and will be in general more susceptible to local defects within the material.

Next, we turn into the details of the SkC dynamics. Figure 3a illustrates the principle for time-evolved REXS measurements. Upon applying a g_x that exceeds the threshold value, the lattices start to roll. The local defects subsequently break the large lattices into pieces of SkCs with, on average, similar sizes.[31,36,40,43,54] Consequently, blocks of SkCs behave like rigid crystallites that travel separately. However, the probing X-rays only measure a fixed local area (20 μm in diameter; Figure 3a), therefore witnessing the iterative events of consecutive SkCs entering and leaving the probed region. In order to obtain the full vision of such complex process, we carried out spatially resolved dynamical REXS measurements.

Figure 3b shows a T-shaped real-space area that is mapped by our time-dependent raster scan. The SkCs are driven for the chosen parameters of $\overline{T}$ = 56.2 K, B_z = 25 mT, and g_x = 0.9 K/mm. At each 20 μm spot, REXS is continuously measured for 500 s before moving to the next neighboring position. As shown in Figure 3b, the mapped area shows three types of rotational behavior, namely, rolling, pinned and mixed

https://doi.org/10.1021/acs.nanolett.4c03336
Nano Lett. 2024, 24, 12226−12232

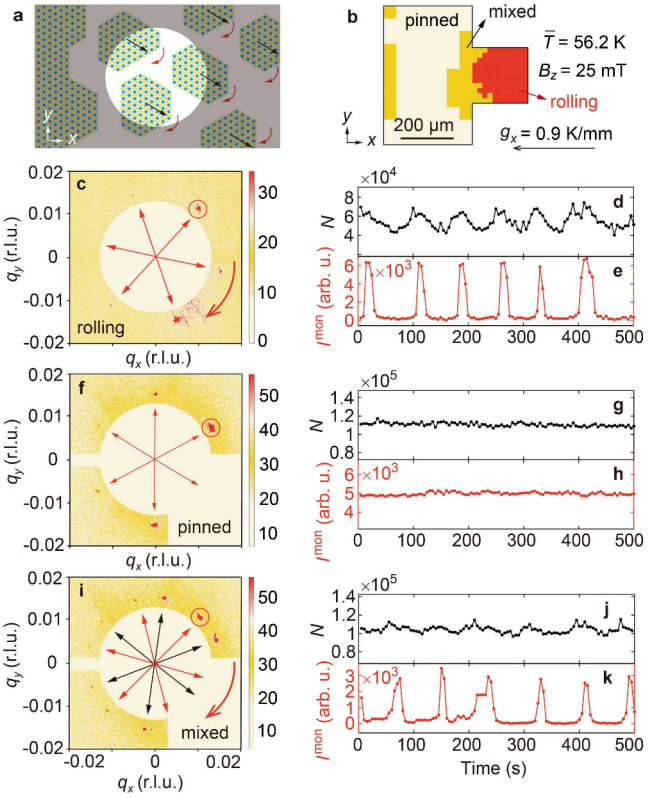

Figure 3. Spatially and time-resolved dynamics. The measurement conditions were $\overline{T}$ = 56.2 K, B_z = 25 mT, g_x = 0.9 K/mm throughout. (a) Illustration of the REXS measurement configuration and the SkC rolling dynamics. The X-ray probing area is highlighted, illustrating the local observation window for the dynamics: Ordered skyrmion lattice patches consecutively enter and leave the monitored area, following a rolling motion. (b) Map of the three dynamic regimes across the sample, i.e., the rolling mode (red), the pinned (light yellow), and the mixed mode (orange). (c) Snapshot of the REXS pattern during the rotation at a typical spot in the rolling region. (d) Plot of the probed total skyrmion number N, and, (e) the locally integrated intensity I^{mon}, as a function of time. The integration area for I^{mon} is indicated by the red circle in (c). Panels (f,g,h) and (i,j,k) show the corresponding data for the pinned and mixed regions, respectively.

dynamics. The complete real-time data can be found in Movies 3−5 in the Supporting Information.

Figure 3c shows a typical snapshot REXS pattern in the rolling region, in which sets of 6-fold-symmetric peaks cycle within the q_x-q_y plane in a clockwise fashion. During the dynamical event, the continuous RSM rotation only sustains for a finite period of time (∼tens of seconds), after which a new set of the 6-fold-symmetric rods suddenly emerge at a different angle. Subsequently, the rotation continues (Movie 6 in the Supporting Information). This indicates that multiple SkCs may travel on a rolling trajectory, consecutively entering and leaving the probing area. To unravel the dynamics in detail, the RSM is quantitatively studied by two types of data analysis. First, we integrate the total magnetic peak intensity I^{tot} for each time step and investigate its time-evolution. It is generally accepted that the total REXS cross-section is proportional to the domain size $N\Omega$ of a SkC,[31,52] thus being linearly proportional to the total skyrmion number, i.e., $I^{tot} = YN$, where the factor Y is an experimentally determined value (Section S1 in the Supporting Information). Thus, by measuring I^{tot}, it is possible to extract the instantaneous skyrmion number N within the probing area. N exhibits an oscillatory profile in time (Figure 3d), suggesting that the translational motions of the SkCs are taking place, which successively enter and leave the observation window.

Second, we define a fixed reciprocal space region at the q_x-q_y plane, which is used to monitor the local peak intensity evolution (red circle in Figure 3c) due to the rotation. If the pattern would rotate, the locally monitored scattering intensity I^{mon} would periodically modulate in time. Figure 3e shows the I^{mon} curve from the same data set as that of Figure 3d, from which the averaged rotation angular velocity ω can be obtained. Combining the dynamic behavior from both N and I^{mon}, it is thus unambiguously clear that the SkCs exhibits both translational and rotational modes under g_x, validating the scenario illustrated in Figure 3a. More importantly, the modulated profiles in N and I^{mon} are loosely correlated in time, which agrees with eq 1 that the angular velocity ω is linearly proportional to the drift velocity v_x.

Moreover, we observed that in certain regions of the sample, the SkC remains static without showing any time dependence (labeled "pinned area" in Figure 3b). Figure 3f shows the dynamical analysis from a typical nonrotating sample area, from which both N and I^{mon} remain unchanged over time. Such static behavior can be ascribed to local structural defects on the surface, which pin the SkCs in place.[43,48] In other words, regions with a higher concentration of structural defects, which serve as strong pinning sites, immobilize the skyrmion crystallites, whereas pinning is negligible in regions with minimal or no structural defects, where and the skyrmion crystallites can move freely. This is evidenced by the spatial overlap of the pinned positions from the raster scan image and the defect positions from the SEM image (Section S4 in the Supporting Information). On the other hand, at the boundary between the pinned area and the rolling region, a mixed dynamical behavior is observed (Figure 3b). Figure 3i shows a typical transient REXS pattern for such a state, in which multiple sets of the 6-fold-symmetric peaks can be found. Note that there is one set of peaks that remains in place without moving (black arrows), while the other keeps rotating (marked in red). This can be further corroborated in the N and I^{mon} profiles in Figure 3j,k. The smooth transition between the pinned and the rolling region further confirms the detailed dynamic modes as predicted by the chiral lattice torque model.

Next, we performed a quantitative analysis to verify the theory. For standard skyrmion dynamics under a thermal gradient, it has been established that the magnon current $j_x \propto g_x$ and the longitudinal velocity $v_x \propto g_x$.[19] Therefore, eq 1 essentially predicts that $\omega \propto g_x^2/N$, i.e., the rotational angular velocity is quadratic in the gradient amplitude and inversely proportional to the total topological number.

Figure 4a shows a plot of ω as a function of g_x measured at $\overline{T}$ = 55.6 K for the averaged SkC with $N \approx 4000$ skyrmions. For small values of g_x below 0.56 K/mm, the SkC motion is locked by structural pinning sites. Upon increasing the amplitude of the gradient above the threshold value, ω follows a quadratic relationship in g_x (red curve in Figure 4a). On the other hand, we observed different rotation events for the same g_x, from which we conclude that SkCs with different sizes exhibit different angular velocities. The $\omega \propto N^{-1}$ relationship can be clearly identified [Figure 4b; red line represents a fit to the data using eq 1]. These results are in excellent agreement

https://doi.org/10.1021/acs.nanolett.4c03336
Nano Lett. 2024, 24, 12226−12232

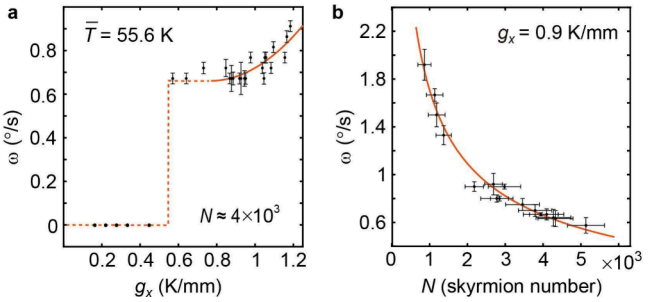

Figure 4. Quantitative analysis of the dynamics based on the chiral lattice torque model. (a) Plot of the SkC rotation angular velocity ω as a function of the magnitude of the gradient, measured at $\bar{T}$ = 55.6 K at a fixed position (in the rolling region shown in Figure 3b). Upon changing the value of g_x, the total skyrmion number remains to be ~4000± 450. Note that g_x cannot exceed 1.2 K/mm, as a larger value would take the local sample temperature outside of the narrow window of the SkL phase pocket. (b) Plot of ω as a function of the total skyrmion number for a fixed value of the gradient of 0.9 K/mm. The red curves are fits to the data based on eq 1.

with the chiral lattice torque model. We estimate that for Cu_2OSeO_3, a typical SkC with $N \approx 4000$ skyrmions experiences a torque of $\Gamma \approx 2.74 \times 10^{-25}$ N ·m under a minute temperature gradient of 0.9 K/mm.

The dynamical properties of skyrmions are of great importance for their manipulation—an active field of research with great relevance for potential technological applications. We identify that the equilibrium SkL phase, in which the quasiparticles are closely packed into a crystal and which can be regarded as a condensed phase of topological matter, is fundamentally different from isolated skyrmions. A direct consequence of this particle ordering is the rigidity of the system, presenting an intrinsic rotational mode, whose dynamics is governed by the chiral lattice torque model. Our temporally and spatially resolved REXS measurements under a linear thermal gradient verified the model, revealing a new rotational degree of freedom for the manipulation of skyrmions. Finally, the continuous rolling motion of a SkC is not restricted to thermal gradient drives alone, but is also attainable via any general linear stimulus gradient, e.g., electric field, strain, electric current, and more.

■ ASSOCIATED CONTENT

Data Availability Statement

All data needed to evaluate the conclusions in the paper are present in the paper and/or the Supporting Information where source data in the form of CCD camera movies are provided. Additional data related to this paper may be requested from the authors.

Supporting Information

The Supporting Information is available free of charge at https://pubs.acs.org/doi/10.1021/acs.nanolett.4c03336.

Materials and methods, the relationship between REXS intensity and skyrmion number, the characteristic REXS signatures for the different dynamic scenarios, the dynamics of the metastable skyrmion lattice phase, and the sample morphology (PDF)

Movies as described in the text (ZIP)

■ AUTHOR INFORMATION

Corresponding Authors

Yizhou Liu − *Anhui Province Key Laboratory of Low-Energy Quantum Materials and Devices, High Magnetic Field Laboratory, HFIPS, Chinese Academy of Sciences, Hefei, Anhui 230031, China*; Email: yzliu@hmfl.ac.cn

Shilei Zhang − *School of Physical Science and Technology, ShanghaiTech University, Shanghai 200031, China; ShanghaiTech Laboratory for Topological Physics and Center for Transformative Science, ShanghaiTech University, Shanghai 200031, China*; orcid.org/0000-0002-6870-9222; Email: shilei.zhang@shanghaitech.edu.cn

Authors

Haonan Jin − *School of Physical Science and Technology, ShanghaiTech University, Shanghai 200031, China; ShanghaiTech Laboratory for Topological Physics, ShanghaiTech University, Shanghai 200031, China*

Jingyi Chen − *School of Physical Science and Technology, ShanghaiTech University, Shanghai 200031, China*; orcid.org/0009-0008-9002-6322

Gerrit van der Laan − *Diamond Light Source, Harwell Science and Innovation Campus, Didcot OX11 0DE, United Kingdom*; orcid.org/0000-0001-6852-2495

Thorsten Hesjedal − *Clarendon Laboratory, Department of Physics, University of Oxford, Oxford OX1 3PU, United Kingdom*; orcid.org/0000-0001-7947-3692

Complete contact information is available at: https://pubs.acs.org/10.1021/acs.nanolett.4c03336

Notes

The authors declare no competing financial interest.

■ ACKNOWLEDGMENTS

This work was supported by the National Key R&D Program of China under contract number 2022YFA1403602 and 2020YFA0309400, the Science and Technology Commission of the Shanghai Municipality (21JC1405100), the National Natural Science Foundation of China (Grant nos. 12074257 and 12241406), and the Double First-Class Initiative Fund of ShanghaiTech University. The resonant soft x-ray scattering experiments were carried out on the RASOR diffractometer at beamline I10 at the Diamond Light Source (Didcot, UK) under proposals MM32087-1 and MM32301-1.

■ REFERENCES

(1) Bogdanov, A. N.; Yablonskii, D. A. Thermodynamically stable 'vortices' in magnetically ordered crystals. The mixed state of magnets. *Sov. Phys. JETP* **1989**, *68*, 101.

(2) Mühlbauer, S.; Binz, B.; Jonietz, F.; Pfleiderer, C.; Rosch, A.; Neubauer, A.; Georgii, R.; Böni, P. Skyrmion Lattice in a Chiral Magnet. *Science* **2009**, *323*, 915.

(3) Nagaosa, N.; Tokura, Y. Topological properties and dynamics of magnetic skyrmions. *Nat. Nanotechnol.* **2013**, *8*, 899.

(4) Volovik, G. E. Linear momentum in ferromagnets. *J. Phys. C: Solid State Phys.* **1987**, *20*, L83.

(5) Zang, J.; Mostovoy, M.; Han, J. H.; Nagaosa, N. Dynamics of Skyrmion Crystals in Metallic Thin Films. *Phys. Rev. Lett.* **2011**, *107*, 136804.

(6) Schulz, T.; Ritz, R.; Bauer, A.; Halder, M.; Wagner, M.; Franz, C.; Pfleiderer, C.; Everschor, K.; Garst, M.; Rosch, A. Emergent electrodynamics of skyrmions in a chiral magnet. *Nat. Phys.* **2012**, *8*, 301−304.

(7) Nagaosa, N.; Tokura, Y. Emergent electromagnetism in solids. *Phys. Scr.* **2012**, *T146*, 014020.
(8) Sampaio, J.; Cros, V.; Rohart, S.; Thiaville, A.; Fert, A. Nucleation, stability and current-induced motion of isolated magnetic skyrmions in nanostructures. *Nat. Nanotechnol.* **2013**, *8*, 839.
(9) Iwasaki, J.; Mochizuki, M.; Nagaosa, N. Current-induced skyrmion dynamics in constricted geometries. *Nat. Nanotechnol.* **2013**, *8*, 742.
(10) Jiang, W.; Upadhyaya, P.; Zhang, W.; Yu, G.; Jungfleisch, M. B.; Fradin, F. Y.; Pearson, J. E.; Tserkovnyak, Y.; Wang, K. L.; Heinonen, O.; te Velthuis, S. G. E.; Hoffmann, A. Blowing magnetic skyrmion bubbles. *Science* **2015**, *349*, 283−286.
(11) Maccariello, D.; Legrand, W.; Reyren, N.; Garcia, K.; Bouzehouane, K.; Collin, S.; Cros, V.; Fert, A. Electrical detection of single magnetic skyrmions in metallic multilayers at room temperature. *Nat. Nanotechnol.* **2018**, *13*, 233.
(12) Thiele, A. A. Steady-State Motion of Magnetic Domains. *Phys. Rev. Lett.* **1973**, *30*, 230.
(13) Jonietz, F.; Mühlbauer, S.; Pfleiderer, C.; Neubauer, A.; Münzer, W.; Bauer, A.; Adams, T.; Georgii, R.; Böni, P.; Duine, R. A.; Everschor, K.; Garst, M.; Rosch, A. Spin Transfer Torques in MnSi at Ultralow Current Densities. *Science* **2010**, *330*, 1648.
(14) Yu, X. Z.; Kanazawa, N.; Zhang, W. Z.; Nagai, T.; Hara, T.; Kimoto, K.; Matsui, Y.; Onose, Y.; Tokura, Y. Skyrmion flow near room temperature in an ultralow current density. *Nat. Commun.* **2012**, *3*, 988.
(15) Iwasaki, J.; Mochizuki, M.; Nagaosa, N. Universal current-velocity relation of skyrmion motion in chiral magnets. *Nat. Commun.* **2013**, *4*, 1463.
(16) Yu, X. Z.; Morikawa, D.; Nakajima, K.; Shibata, K.; Kanazawa, N.; Arima, T.; Nagaosa, N.; Tokura, Y. Motion tracking of 80-nm-size skyrmions upon directional current injections. *Sci. Adv.* **2020**, *6*, No. eaaz9744.
(17) Wang, W.; Song, D.; Wei, W.; Nan, P.; Zhang, S.; Ge, B.; Tian, M.; Zang, J.; Du, H. Electrical manipulation of skyrmions in a chiral magnet. *Nat. Commun.* **2022**, *13*, 1593.
(18) Song, D.; Wang, W.; Zhang, S.; Liu, Y.; Wang, N.; Zheng, F.; Tian, M.; Dunin-Borkowski, R. E.; Zang, J.; Du, H. Steady motion of 80-nm-size skyrmions in a 100-nm-wide track. *Nat. Commun.* **2024**, *15*, 5614.
(19) Kong, L.; Zang, J. Dynamics of an Insulating Skyrmion under a Temperature Gradient. *Phys. Rev. Lett.* **2013**, *111*, 067203.
(20) Lin, S.-Z.; Reichhardt, C.; Batista, C. D.; Saxena, A. Particle model for skyrmions in metallic chiral magnets: Dynamics, pinning, and creep. *Phys. Rev. B* **2013**, *87*, 214419.
(21) Lin, S.; Batista, C. D.; Reichhardt, C.; Saxena, A. ac current generation in chiral magnetic insulators and skyrmion motion induced by the spin Seebeck effect. *Phys. Rev. Lett.* **2014**, *112*, 187203.
(22) Mochizuki, M.; Yu, X. Z.; Seki, S.; Kanazawa, N.; Koshibae, W.; Zang, J.; Mostovoy, M.; Tokura, Y.; Nagaosa, N. Thermally driven ratchet motion of a skyrmion microcrystal and topological magnon Hall effect. *Nat. Mater.* **2014**, *13*, 241.
(23) Zázvorka, J.; Jakobs, F.; Heinze, D.; Keil, N.; Kromin, S.; Jaiswal, S.; Litzius, K.; Jakob, G.; Virnau, P.; Pinna, D.; Everschor-Sitte, K.; Rózsa, L.; Donges, A.; Nowak, U.; Kläui, M. Thermal skyrmion diffusion used in a reshuffler device. *Nat. Nanotechnol.* **2019**, *14*, 658.
(24) Wang, Z.; et al. Thermal generation, manipulation and thermoelectric detection of skyrmions. *Nat. Electron.* **2020**, *3*, 672.
(25) Litzius, K.; et al. The role of temperature and drive current in skyrmion dynamics. *Nat. Electron.* **2020**, *3*, 30.
(26) Yu, X.; Kagawa, F.; Seki, S.; Kubota, M.; Masell, J.; Yasin, F. S.; Nakajima, K.; Nakamura, M.; Kawasaki, M.; Nagaosa, N.; Tokura, Y. Real-space observations of 60-nm skyrmion dynamics in an insulating magnet under low heat flow. *Nat. Commun.* **2021**, *12*, 5079.
(27) Gong, C.; Zhou, Y.; Zhao, G. Dynamics of magnetic skyrmions under temperature gradients. *Appl. Phys. Lett.* **2022**, *120*, 052402.
(28) Raimondo, E.; Saugar, E.; Barker, J.; Rodrigues, D.; Giordano, A.; Carpentieri, M.; Jiang, W.; Chubykalo-Fesenko, O.; Tomasello, R.; Finocchio, G. Temperature-Gradient-Driven Magnetic Skyrmion Motion. *Phys. Rev. Appl.* **2022**, *18*, 024062.
(29) Qin, G.; Zhang, X.; Zhang, R.; Pei, K.; Yang, C.; Xu, C.; Zhou, Y.; Wu, Y.; Du, H.; Che, R. Dynamics of magnetic skyrmions driven by a temperature gradient in a chiral magnet FeGe. *Phys. Rev. B* **2022**, *106*, 024415.
(30) Vogel, M.; Zimmermann, B.; Wild, J.; Schwarzhuber, F.; Mewes, C.; Mewes, T.; Zweck, J.; Back, C. H. Driving a magnetic texture by magnon currents. *Phys. Rev. B* **2023**, *107*, L100409.
(31) Zhang, S. L.; Wang, W. W.; Burn, D. M.; Peng, H.; Berger, H.; Bauer, A.; Pfleiderer, C.; van der Laan, G.; Hesjedal, T. Manipulation of skyrmion motion by magnetic field gradients. *Nat. Commun.* **2018**, *9*, 2115.
(32) Psaroudaki, C.; Loss, D. Skyrmions Driven by Intrinsic Magnons. *Phys. Rev. Lett.* **2018**, *120*, 237203.
(33) Seki, S.; Yu, X. Z.; Ishiwata, S.; Tokura, Y. Observation of Skyrmions in a Multiferroic Material. *Science* **2012**, *336*, 198.
(34) Adams, T.; Mühlbauer, S.; Pfleiderer, C.; Jonietz, F.; Bauer, A.; Neubauer, A.; Georgii, R.; Böni, P.; Keiderling, U.; Everschor, K.; Garst, M.; Rosch, A. Long-Range Crystalline Nature of the Skyrmion Lattice in MnSi. *Phys. Rev. Lett.* **2011**, *107*, 217206.
(35) Adams, T.; Chacon, A.; Wagner, M.; Bauer, A.; Brandl, G.; Pedersen, B.; Berger, H.; Lemmens, P.; Pfleiderer, C. Long-Wavelength Helimagnetic Order and Skyrmion Lattice Phase in Cu_2OSeO_3. *Phys. Rev. Lett.* **2012**, *108*, 237204.
(36) Zhang, S. L.; Bauer, A.; Burn, D. M.; Milde, P.; Neuber, E.; Eng, L. M.; Berger, H.; Pfleiderer, C.; van der Laan, G.; Hesjedal, T. Multidomain Skyrmion Lattice State in Cu_2OSeO_3. *Nano Lett.* **2016**, *16*, 3285−3291.
(37) Rößler, U. K.; Leonov, A. A.; Bogdanov, A. N. Chiral Skyrmionic matter in non-centrosymmetric magnets. *J. Phys.: Conf. Ser.* **2011**, *303*, 012105.
(38) Leonov, A. O.; Monchesky, T. L.; Loudon, J. C.; Bogdanov, A. N. Three-dimensional chiral skyrmions with attractive interparticle interactions. *J. Phys.: Cond. Matter* **2016**, *28*, 35LT01.
(39) Du, H.; Zhao, X.; Rybakov, F. N.; Borisov, A. B.; Wang, S.; Tang, J.; Jin, C.; Wang, C.; Wei, W.; Kiselev, N. S.; Zhang, Y.; Che, R.; Blugel, S.; Tian, M. Interaction of Individual Skyrmions in Nanostructured Cubic Chiral Magnet. *Phys. Rev. Lett.* **2018**, *120*, 197203.
(40) Pöllath, S.; Wild, J.; Heinen, L.; Meier, T. N. G.; Kronseder, M.; Tutsch, L.; Bauer, A.; Berger, H.; Pfleiderer, C.; Zweck, J.; Rosch, A.; Back, C. H. Dynamical Defects in Rotating Magnetic Skyrmion Lattices. *Phys. Rev. Lett.* **2017**, *118*, 207205.
(41) Yu, X.; Morikawa, D.; Yokouchi, T.; Shibata, K.; Kanazawa, N.; Kagawa, F.; Arima, T.; Tokura, Y. Aggregation and collapse dynamics of skyrmions in a non-equilibrium state. *Nat. Phys.* **2018**, *14*, 832.
(42) Tang, J.; Wu, Y.; Wang, W.; Kong, L.; Lv, B.; Wei, W.; Zang, J.; Tian, M.; Du, H. Magnetic skyrmion bundles and their current-driven dynamics. *Nat. Nanotechnol.* **2021**, *16*, 1086.
(43) Reichhardt, C.; Reichhardt, C. J. O.; Milosevic, M. V. Statics and dynamics of skyrmions interacting with disorder and nanostructures. *Rev. Mod. Phys.* **2022**, *94*, 035005.
(44) Landau, L. D. On The Theory of Phase Transitions. *Zh. Eksp. Teor. Fiz.* **1937**, *7*, 19.
(45) Chaikin, P. M.; Lubensky, T. C. *Principles of Condensed Matter Physics*; Cambridge University Press: 1995.
(46) Blundell, S. J. *Magnetism in Condensed Matter*; Oxford University Press: 2001.
(47) Everschor, K.; Garst, M.; Duine, R. A.; Rosch, A. Current-induced rotational torques in the skyrmion lattice phase of chiral magnets. *Phys. Rev. B* **2011**, *84*, 064401.
(48) Everschor, K.; Garst, M.; Binz, B.; Jonietz, F.; Mühlbauer, S.; Pfleiderer, C.; Rosch, A. Rotating skyrmion lattices by spin torques and field or temperature gradients. *Phys. Rev. B* **2012**, *86*, 054432.
(49) Leonov, A. O.; Bogdanov, A. N. Crossover of skyrmion and helical modulations in noncentrosymmetric ferromagnets. *New J. Phys.* **2018**, *20*, 043017.

https://doi.org/10.1021/acs.nanolett.4c03336
Nano Lett. 2024, 24, 12226−12232

(50) Jiang, W.; Zhang, X.; Yu, G.; Zhang, W.; Wang, X.; Benjamin Jungfleisch, M.; Pearson, J. E.; Cheng, X.; Heinonen, O.; Wang, K. L.; Zhou, Y.; Hoffmann, A.; te Velthuis, S. G. E. Direct observation of the skyrmion Hall effect. *Nat. Phys.* **2017**, *13*, 162−169.
(51) Litzius, K.; et al. Skyrmion Hall effect revealed by direct time-resolved X-ray microscopy. *Nat. Phys.* **2017**, *13*, 170−175.
(52) Zhang, S. L.; Bauer, A.; Berger, H.; Pfleiderer, C.; van der Laan, G.; Hesjedal, T. Resonant elastic x-ray scattering from the skyrmion lattice in Cu_2OSeO_3. *Phys. Rev. B* **2016**, *93*, 214420.
(53) Rajeswari, J.; Huang, P.; Mancini, G. F.; Murooka, Y.; Latychevskaia, T.; McGrouther, D.; Cantoni, M.; Baldini, E.; White, J. S.; Magrez, A.; Giamarchi, T.; Rønnow, H. M.; Carbone, F. Filming the formation and fluctuation of Skyrmion domains by cryo-Lorentz transmission electron microscopy. *Proc. Natl. Acad. Sci. U.S.A.* **2015**, *112*, 14212.
(54) Zhang, S. L.; Bauer, A.; Berger, H.; Pfleiderer, C.; van der Laan, G.; Hesjedal, T. Imaging and manipulation of skyrmion lattice domains in Cu_2OSeO_3. *Appl. Phys. Lett.* **2016**, *109*, 192406.
(55) Ran, K.; Liu, Y.; Guang, Y.; Burn, D. M.; van der Laan, G.; Hesjedal, T.; Du, H.; Yu, G.; Zhang, S. Creation of a Chiral Bobber Lattice in Helimagnet-Multilayer Heterostructures. *Phys. Rev. Lett.* **2021**, *126*, 017204.
(56) Jin, H.; Tan, W.; Liu, Y.; Ran, K.; Fan, R.; Shangguan, Y.; Guang, Y.; van der Laan, G.; Hesjedal, T.; Wen, J.; Yu, G.; Zhang, S. Evolution of Emergent Monopoles into Magnetic Skyrmion Strings. *Nano Lett.* **2023**, *23*, 5164.
(57) Beale, T. A. W.; Hase, T. P. A.; Iida, T.; Endo, K.; Steadman, P.; Marshall, A. R.; Dhesi, S. S.; van der Laan, G.; Hatton, P. D. RASOR: an advanced instrument for soft x-ray reflectivity and diffraction. *Rev. Sci. Instrum.* **2010**, *81*, 073904.
(58) Zhang, S. L.; van der Laan, G.; Wang, W. W.; Haghighirad, A. A.; Hesjedal, T. Direct Observation of Twisted Surface skyrmions in Bulk Crystals. *Phys. Rev. Lett.* **2018**, *120*, 227202.
(59) Zhang, S.; van der Laan, G.; Müller, J.; Heinen, L.; Garst, M.; Bauer, A.; Berger, H.; Pfleiderer, C.; Hesjedal, T. Reciprocal space tomography of 3D skyrmion lattice order in a chiral magnet. *Proc. Natl. Acad. Sci. U.S.A.* **2018**, *115*, 6386−6391.
(60) Oike, H.; Kikkawa, A.; Kanazawa, N.; Taguchi, Y.; Kawasaki, M.; Tokura, Y.; Kagawa, F. Interplay between topological and thermodynamic stability in a metastable magnetic skyrmion lattice. *Nat. Phys.* **2016**, *12*, 62.

https://doi.org/10.1021/acs.nanolett.4c03336
Nano Lett. 2024, 24, 12226−12232